Journal of Neuroinflammation

RESEARCH Open Access

Ganglion cell-derived LysoPS induces retinal neovascularisation by activating the microglial GPR34-PI3K-AKT-NINJ1 axis

Lushu Chen[1,2], HuiYing Zhang[1,2], Ying Zhang[1,2], Xiumiao Li[1], MeiHuan Wang[1], Yaming Shen[1], Yuan Cao[2], Yong Xu[1,2*] and Jin Yao[1,2*]

Abstract

Retinal neovascularisation is a major cause of blindness in patients with proliferative diabetic retinopathy (PDR). It is mediated by the complex interaction between dysfunctional ganglion cells, microglia, and vascular endothelial cells. Notably, retinal microglia, the intrinsic immune cells of the retina, play a crucial role in the pathogenesis of retinopathy. In this study, we found that lysophosphatidylserines (LysoPS) released from injured ganglion cells induced microglial extracellular trap formation and retinal neovascularisation. Mechanistically, LysoPS activated the GPR34-PI3K-AKT-NINJ1 signalling axis by interacting with the GPR34 receptor on the microglia. This activation upregulated the expression of inflammatory cytokines, such as IL-6, IL-8, VEGFA, and FGF2, and facilitated retinal vascular endothelial cell angiogenesis. As a result, inhibition of the GPR34-PI3K-AKT-NINJ1 axis significantly decreased microglial extracellular trap formation and neovascularisation by suppressing LysoPS-induced microglial inflammatory responses, both in vitro and in vivo. This study reveals the crucial role of apoptotic ganglion cells in activating microglial inflammation in PDR, thereby enhancing our understanding of the pathogenesis of retinal neovascularisation.

Keywords LysoPS, GPR34, PI3K-AKT, NINJ1, Microglial extracellular traps, Retinal neovascularisation

Introduction

Pathological neovascularisation is a primary cause of vision loss, characterised by the formation of neovascular lacking tight junctions [1]. Common retinal neovascularisation diseases include diabetic retinopathy (DR), retinopathy of prematurity, and retinal vein occlusion. Among these diseases, proliferative diabetic retinopathy (PDR) is the most prevalent in terms of onset [2–4]. Diabetes mellitus, characterised by hyperglycemia and glucose intolerance, often leads to significant damage to various body systems, particularly the vascular and nervous systems. DR, a prevalent ocular complication in diabetic patients, manifests as a neurovascular disorder characterised by microvascular dysfunction and neurodegeneration [5]. In its early stages, the disease is characterised by retinal vascular degeneration and decreased retinal perfusion [6]. The retina mainly comprises energy-intensive neurons, including rod, cone, and ganglion cells, which are highly susceptible to changes in blood supply [7, 8]. To compensate for the degeneration caused by DR, retinal neurons adaptively stimulate retinal

*Correspondence:
Yong Xu
yxu4696@njmu.edu.cn
Jin Yao
dryaojin@126.com
[1]The Affiliated Eye Hospital, Nanjing Medical University, 138 Hanzhong Road, Nanjing 210029, P. R. China
[2]The Fourth School of Clinical Medicine, Nanjing Medical University, 140 Hanzhong Road, Nanjing 210029, P. R. China

neovascularisation to meet their nutrient and oxygen requirements. However, this compensatory mechanism leads to several detrimental effects, including fibrovascular membrane formation, which exerts excessive traction on the retina due to impaired pericyte function. The pericytes fail to adequately cover the vascular wall, compromising vessel integrity and leading to increased vascular permeability, ultimately resulting in leakage, bleeding, and reduction in visual acuity [9, 10].

Targeted vascular endothelial growth factor (VEGF) therapy has been widely used to manage neovascularisation in DR patients [5, 11]. However, its efficacy is limited over time due to the development of drug resistance, often arising from the multiple treatment injections required during treatment [12]. Given these challenges, there is an urgent need to develop alternative approaches for managing neovascularisation in DR. It is well established that DR results from chronic dysfunction in the retinal neurovascular unit, comprising neurons, microglia, and the vascular system [8]. Notably, microglia serve as critical intermediaries between neurons and blood vessels, performing immunosurveillance and clearance functions, such as removing cell debris, pathogens, and damaged or dying cells to maintain retinal homeostasis [13, 14]. However, microglia hyperactivation contributes to the onset of pathologic neovascularisation [15].

Emerging evidence demonstrated that inflammation induces microglia to undergo extracellular trapping, a phenomenon first discovered in neutrophils and characterised as a novel form of programmed cell death termed 'ETosis' [16–18]. ETosis is driven by distinct cellular events, including cytoskeleton and nuclear membrane disintegration, chromatic decondensation assembly of antifungal proteins on chromatin scaffolds, and plasma membrane rupture [19, 20]. Extracellular trap is present not only in neutrophils but also in other cells, such as mast cells, eosinophils, and basophils [16, 21, 22]. The interplay between nuclear materials and cellular proteins in chromatin plays a crucial role in the progression of various diseases, including rheumatoid arthritis, sepsis, and thrombosis [23–25].

Lysophosphatidylserine (LysoPS) is a lysophospholipid formed by the action of phosphatidylserine phospholipase A (PLA) on the membrane of activated or apoptotic cells and is now considered a crucial factor in initiating autoimmune disorders [26]. Studies have shown that LysoPS is essential for neuronal development by interacting with microglia, although the underlying mechanism is not yet fully understood [27]. Despite its potential role in neuronal development, we predict that excessive LysoPS interaction with microglia may contribute to retinal angiogenesis. Therefore, this study investigated the role of LysoPS in microglial extracellular trapping and its effect on retinal neovascularisation through both ex vivo and in vivo approaches.

Materials and methods

Patients

Following the Declaration of Helsinki, the Nanjing Medical University Affiliated Eye Hospital collected vitreous fluids and fibrovascular membrane samples from eight patients with PDR and eight patients with proliferative vitreoretinopathies (PVR). The clinical study protocol was approved by the Ethical Committee of Nanjing Medical University, and written informed consent was obtained from all participants to ensure they fully understood the study's purpose and procedures. First, a 0.1-ml sample of pure vitreous humour was collected from each patient using a sterile syringe under a surgical microscope before vitrectomy. Subsequently, the samples were centrifuged at 1000 rpm for 15 min at 4 °C to remove tissue debris from the vitreous fluid and stored at −80 °C for further analysis.

Mice

To establish the mouse oxygen-induced retinopathy (OIR) experimental model, neonatal C57BL/6 mice (Ziyuan Experimental Animal, China) were kept in room air with 21% oxygen for seven days and then exposed to 75% oxygen for five days, along with their nursing mothers. Following hypertoxic stimulation, the mice were returned to room air (21% oxygen) and maintained for five days to induce retinal neovascularisation. Subsequently, the mice were intravitreally injected with 1 μl of AAV-carried shRNA (2.2×10^{12} vg/ml) to specifically silence NINJ1 (GeneChem, China) in the retina. Simultaneously, they were intravitreally injected with 1 μl of 10 μM LysoPS (0130549, Aladdin, USA), 5 μM GPR34 antagonist (HY-138501, MedChemExpress, USA), or 10 μM PI3K inhibitor LY294002 (HY-10108, MedChemExpress). Neovascular and avascular areas were quantified using Image J (NIH), and the results were expressed as percentages of the total retinal area.

Retinal imaging

Mouse eyes were excised and immediately fixed in 4% paraformaldehyde for 1 h. After removing the anterior neuroretina, the retinas were dissected into petal-shaped pieces for whole flat-mount preparation. Following 15 min of incubation in 4% PFA, the retinal slides were blocked in 1 × PBS containing 5% BSA and 1% Triton X-100 for 1 h, then incubated overnight at 4 °C with primary antibodies against Isolectin B4 (IB4) (1:50, L2895, Sigma, USA). The slides were subsequently washed with PBST three times and imaged using a fluorescence microscope (Olympus IX 73 DP80, Japan). Next, the excised eye samples were cryoprotected in 1 × PBS containing

30% sucrose for 48 h. The eyecups were embedded, and 10-mm tissue sections were obtained using a frozen microtome (Thermo Scientific, USA). After blocking for 1 h, the sections were incubated overnight at 4 °C with rabbit NINJ1 antibody (1:200, bs-11105R, Bioss, USA), rabbit IBA1 antibody (1:100, ET1705-78, Wako, Japan), and rabbit CITH3 antibody (1:300, ab5103, Abcam, UK), and followed by incubation with fluorophore-conjugated secondary antibody for 2 h at room temperature. Finally, incubated sections were counterstained with DAPI and visualized using a fluorescence microscope (Olympus IX 73 DP80, Japan).

Primary cell culture

Primary retinal ganglion cells were isolated from three-day-old mouse pups. Briefly, the pups were euthanized, and their eyes were enucleated. The retinas were then carefully dissected from the underlying retinal pigment epithelium layer. The dissected retinas were dissociated with 15 U/ml papain solution (HY-P1645, MedChemExpress) and 70 U/ml collagenase (P45762, MedChemExpress) for 15 min. The digestion process was terminated by adding FBS to the solution. The resulting cell suspension was filtered through a 70 μm filter to remove tissue debris and then centrifuged at 1000 rpm for 10 min. The cell pellet was resuspended and cultured in a ganglion cell-conditioned medium (CM-M122, Priscilla Biotechnology, China). The retinal ganglion cells were identified by staining with an antibody against Tuj1 (ab78078, Abcam).

Bone marrow-derived macrophages (BMDM) were isolated from 4–6-week-old C57BL/6 mice. Following euthanasia, the femurs and tibias of the mice were excised, and bone marrow cells were harvested and centrifuged at 1200 rpm for 5 min to remove debris. After removing the supernatants, 2 ml red blood cell lysis buffer (ab204733, Abcam) was added to the cell pellet for 5 min to lyse the erythrocytes, followed by centrifugation at 1200 rpm for another 5 min. The resuspended cell pellets were cultured in DMEM for 12 h to remove stromal cells, including fibroblasts. The non-adherent cells were collected by centrifugation at 1200 rpm for 4 min and cultured in DMEM supplemented with 10% heat-inactivated FBS (Life Tech., USA), 1% penicillin-streptomycin (15140122, Thermo Sci., USA), and 10 ng/mL recombinant mouse M-CSF (315-02, PeproTech, USA) for 3–4 days to induce macrophage differentiation.

Sprouting assay

Choroidal explants containing the retinal pigment epithelium, choroid, and sclera complex were dissected from three-week-old mice. The peripheral areas of these choroidal explants were isolated and cut into small pieces measuring 0.5×0.5 mm. These explants were immediately embedded in 40 μl growth factor-reduced Matrigel (354,230, Corning, USA) in 24-well tissue culture plates. The embedded explants were cultured in 0.5 ml DMEM for three days, and then 0.5 ml supernatant collected from BMDM primary culture was added to each well. Endothelial sprouts were visualized using a fluorescence microscope (Olympus, Japan), and the sprouting areas were quantified using Image J. Additionally, fibrovascular membrane (FVM) was collected from PDR patients and cut into 0.5×0.5 mm pieces. The FVM explants were grown in 0.5 ml endothelial cell-specific medium supplemented with 12% FBS and then co-cultured with HMC3 cell supernatants. The endothelial sprouts from the FVM explants were imaged and quantified using Image J.

Oxygen-glucose deprivation

Oxygen-glucose deprivation was employed to stimulate retinal hypoxic conditions. The primary retinal ganglion cells (RGCs) were briefly cultured in a glucose-free medium and subjected to hypoxia (1% O_2 and 95% N_2) for 18 h. The cells were then returned to standard culture conditions for 24 h. Cytotoxicity was quantified using a TUNEL assay (C1086, Beyotime, China).

Cell treatment

The HMC3 cell line was purchased from Procell Life Science & Technology, China, and the HRVEC cell line was provided by the Cell Bank of the National Academy of Science, China. Both cell lines were cultured in DMEM supplemented with 10% or 12% FBS. To determine the effect of NINJ1, HMC3 cells were infected with a lentiviral vector carrying shRNA targeting NINJ1. HMC3 and NINJ1-silenced HMC3 cells were treated with dose-escalated LysoPS (0–24 μM) for 9 h. To inhibit LysoPS-induced inflammation, the cells were further treated with 2 μM GPR34 antagonist or 5 μM LY294002. After treatment, the medium was replaced, and cells were rinsed with 1 × PBS thrice to remove these reagents. After continuous culture for 12 h, cell supernatants were collected, filtered through 0.22 μm filters to remove cell debris, and then cocultured with HRVEC cells for 24 h to assess cell angiogenesis.

Cell proliferation

Cell proliferation was determined using the Beyo-Click EdU detection kit (C0071S, Beyotime, China). In brief, the cells were incubated with 50 mM of EdU for 4 h and then fixed in 4% PFA for 15 min. After washing three times with 5% BSA, cells were blocked with 0.3% Triton X-100 for 15 min and incubated with a reaction solution for 30 min in the dark. Cell nuclei were stained with DAPI to ensure an equal number of cells were plated. EdU images were captured using an Olympus IX-73 microscope, and cell proliferation was evaluated

by calculating the percentage of EdU-positive cells using Image J.

Cell migration

Cell migration was analysed using a transwell assay (3422, Corning). After coculturing with microglial supernatants, 5×10^4 HRVEC cells were seeded into the upper chambers containing 200 µl of serum-free medium, while the lower chambers were filled with 500 µl of the regular medium. Cells on the inserts were fixed with 4% PFA for 15 min and then stained with 0.1% crystal violet solution for 3 min. Migrated cells were captured using a light microscope.

Cell tube formation

To solidify matrix gel, each well of the 24-well plates was coated with 40 µl growth factor-reduced Matrigel (354230, Corning) and allowed to polymerize at 37 °C for 45 min. HRVEC cells (2×10^5 cells/well) were then seeded onto the solidified matrix gel for 6 h. Tube formation was visualized using an Olympus IX-73 microscope, and the tube formation ability was analysed by calculating the tube length using Image J.

RT-qPCR

Total RNA was extracted from cells and tissues using Trizol Reagent (15596018CN, Thermo Sci.) and converted into cDNAs using the SuperScript IV First-Strand Synthesis System (R412-01, Vazyme, China). cDNAs were quantified by qPCR with gene-specific primers using a PowerUp SYBR Green Master Mix (Q111-02, Vazyme, China). The mRNA levels were quantified by normalizing to β-actin. The primer sequences for NINJ1: forward primer, 5'-GTCGGGCACTGAGGAGTAT-3', reverse primer, 5'-TTTACATTGATGGGCCGGTT-3'; for GPR34: forward primer, CTCCCACAGAATGCGCTTTAT, reverse primer, CAACCAGTCCCACGATGAAA; for GPR174: forward primer, TTGGTTTCTCATGTACCCCTTTCGC, reverse primer, AACCGTCTTCCAGGTACAATATAGGACA; for p2ry10: forward primer, CTGGAAGCGTAGGTACGATGT, reverse primer, CGACCAACGCAACTGCATT; for β-actin: forward primer, 5'-GGCTGTATTCCCCTCCATCG-3', reverse primer, 5'-CCAGTTGGTAACAATGCCATGT-3'.

Crosslinking

LysoPS-treated HMC3 cells were incubated with 1 mM BS3 crosslinker (21580, Thermo Sci.) for 5 min, followed by incubation with 20 mM Tris (pH 7.5) for 15 min to stop the crosslinking reaction. The culture supernatants were then obtained to detect relevant proteins using immunoblotting.

Immunoblotting

Total protein was extracted from cells and tissues using RIPA buffer (Sigma) supplemented with a 1% protease inhibitor cocktail (Pierce, USA). Equal amounts of the extracted protein (50 µg) were loaded onto an SDS-PAGE gel and transferred to polyvinylidene difluoride membranes. After blocking with 5% milk in TBST for 2 h, the membranes were incubated overnight at 4 °C with the following primary antibodies: rabbit anti-PI3K p85 alpha (1:1000, 4292), rabbit anti-pPI3K p85 alpha (1:1000, 4228), rabbit anti-AKT (1:1000, 4685), rabbit anti-pAKT (1:1000, 4060), rabbit anti-VEGFA (1:1000, 50661), rabbit anti-VEGFR2 (1:1000, 2479), rabbit anti-pVEGFR2 (1:1000, 3770), rabbit anti-STAT3 (1:1000, 9139), rabbit anti-pSTAT3 (1:1000, 9145), and mouse anti-βactin (1:1000, 4967). All antibodies were purchased from Cell Signalling Tech., USA, except mouse anti-NINJ1 (1:1000, sc-136295, Santa Cruz Biotech., USA), The membranes were washed three times in TBST and then incubated with secondary antibodies (1:1000, Thermo Sci.) for 2 h. Immunoblots were visualised using an enhanced chemiluminescence (ECL) kit (WP20005, Thermo Sci.) with the ChemiDoc MP system (Bio-Rad). The intensities of the blots were normalised to β-actin.

ELISA

The protein levels in the vitreous humour, mouse retinal homogenate, and cell supernatants were quantified using relative ELISA kits. Kits for human and mouse LysoPS (MM-62211H1, MM-46962M1, Meimian, China) and mouse IL-8 (EMC104QT, NeoBiosci. Tech., China) were obtained from the specified suppliers, while other kits, including human and mouse IL-6 (EH2IL6, KMC006), human and mouse VEGFA (BMS277-2, BMS619-2), human and mouse FGF2 (KHG0021, EMFGF2), and human IL-8 (88-8086-88) were obtained from Thermo Scientific (USA). Absorbance at 450 nm was measured in triplicate using an automatic flat panel reader (Mol. Devices, USA).

Flow cytometry

Living cells were resuspended in FACS buffer and incubated in 100 µl FACS buffer containing 2 µl Fc block for 10 min. The incubated cells were then stained with FITC anti-mouse CD11b (1:50, 11-0112-82, Thermo Sci.), PE anti-mouse F4/80 (1:50, 111603, BioLegend, USA), and APC anti-human CD31 (1:50, 303115, BioLegend) for 30 min. Stained cells were identified using a BeckMan CytoFlex (BeckMan Coulter, USA).

Statistical analysis

The data from at least three replicates were presented as the mean ± standard deviation (SD). Significant differences between different groups were determined by an

unpaired Student's *t*-test. One-way or two-way analysis of variance (ANOVA) followed by Dunnett's or Bonferroni's multiple comparison tests was performed using Prism (GraphPad, USA). Statistical significance was set at $p < 0.05$.

Results

LysoPS levels are increased in the vitreous fluid of PDR patients and retinal tissues of OIR mice

To quantify LysoPS levels in the eyes of DR patients, vitreous fluids were collected from both PDR and PVR patients. The results showed increased LysoPS levels in PDR patients than in PVR patients (Fig. 1A). In addition, LysoPS levels consistently increased in OIR mice compared to untreated control mice (Fig. 1B). Given the association of LysoPS production with apoptotic cells [27], retinal tissue slices excised from OIR mice were analysed using a TUNEL assay. Notably, a high density of apoptotic cells was detected in the retinal ganglion layer, which suggested that LysoPS was mainly produced from damaged ganglion cells (Fig. 1C, D). The primary RGCs, isolated and characterised by Tuj1 staining (Fig. 1E, F), showed a significant increase in the apoptotic rate under the hypoxic condition (Fig. 1G, H). Similarly, LysoPS levels in the supernatants of primary ganglion cell culture were significantly increased under hypoxia (Fig. 1I). These results suggested that the high levels of LysoPS released from the apoptotic ganglion cells may contribute to the development of PDR.

LysoPS induces microglial extracellular trap formation

Three LysoPS receptors (GPR34, GPR174, and P2Y10) have been identified [28]. To investigate the role of LysoPS in the pathogenesis of PDR, the expression profiles of these receptors were analysed using a bioinformatic database and validated by RT-PCR. The results showed that GPR34 expression was significantly increased in the microglia of PDR patients than in PVR patients (Fig. S1A, B). It is well established that GPR34, a visual purple-like G protein-coupled receptor, is predominantly expressed in neural microglia and facilitates tissue repair by detecting signals indicative of tissue damage [29, 30]. Therefore, to investigate the potential role of LysoPS in inducing microglial extracellular trap formation, human microglial HMC3 cells were treated with dose-escalated LysoPS and stained with SYTOX Green. Although high doses of LysoPS increased cell death, 12 μM LysoPS effectively stimulated extracellular trap formation, as evidenced by nuclear membrane rupture and filamentous DNA (Fig. 2A). Additionally, LysoPS significantly increased the levels of double-stranded DNA (dsDNA) and lactate dehydrogenase (LDH) (Fig. 2B, C). Consistently, the dsDNA level in vitreous fluid from PDR patients was higher than in PVR patients (Fig. 2D). Furthermore, BMDM cells were extracted from mice and characterised using relative markers (Fig. S2A). BMDM is characterized by sharing many phenotypes and functions with microglia and was frequently used as a microglial surrogate to study microglial response [31, 32]. Thus, we isolated BMDM from mice and treated with LysoPS. Similarly, LysoPS induced extracellular traps with high levels of dsDNA and LDH in BMDM cells (Fig. S2 B–D). Notably, citrullinated histone H3 (CITH3), an extracellular trap marker, was colocalised with microglial marker IBA1 in retinal tissues from PDR patients and OIR mice (Fig. 2E, F). The results indicated that LysoPS induced microglia extracellular trap formation by interacting with the GPR34 receptor.

LysoPS induces microglial inflammation by activating the PI3K-AKT signalling and NINJ1

Mounting evidence demonstrated that activation of pro-inflammatory signalling plays a fundamental role in the pathogenesis of DR [9, 13]. To determine if LysoPS triggers microglial extracellular trap through inflammatory activation, the levels of PI3K, AKT, and their phosphorylated forms were quantified in LysoPS-treated HMC3 cells. Expectedly, LysoPS upregulated phosphorylated PI3K-AKT, indicating the involvement of the PI3K-AKT pathway in LysoPS-mediated microglial inflammation (Fig. 3A–C). Additionally, LysoPS significantly increased NINJ1 expression (Fig. 3D, E), a protein implicated in cell membrane rupture and neuronal injury [33, 34]. These findings were consistent with the results from bioinformatic analyses comparing PDR and PVR (Fig. 3F). Furthermore, colocalisation of NINJ1 and microglial marker IBA1 significantly enhanced in retinal tissues from OIR mice compared to the control mice (Fig. 3G). Similarly, the colocalized image was pronounced in the fibrovascular membrane of PDR patients than in PVR patients (Fig. 3H). Additionally, the levels of inflammatory cytokines, including IL6, IL8, VEGFA, and FGF2, were significantly elevated in LysoPS-treated HMC3 cells (Fig. 3I–L). These results indicate that the activation of the PI3K-AKT signalling pathway and the upregulation of NINJ1 are crucial mechanisms underlying LysoPS-induced inflammatory response and microglial extracellular trap formation.

LysoPS fosters microglia-mediated endothelial angiogenesis

To determine the effect of LysoPS-induced microglia inflammation on retinal neovascularisation, supernatants from LysoPS-treated HMC3 cells were cocultured with human retinal vascular endothelial cells (HRVEC). As shown in Fig. 4A–D, LysoPS significantly enhanced endothelial cell proliferation, migration, and tube formation. Furthermore, mice-derived choroid membranes

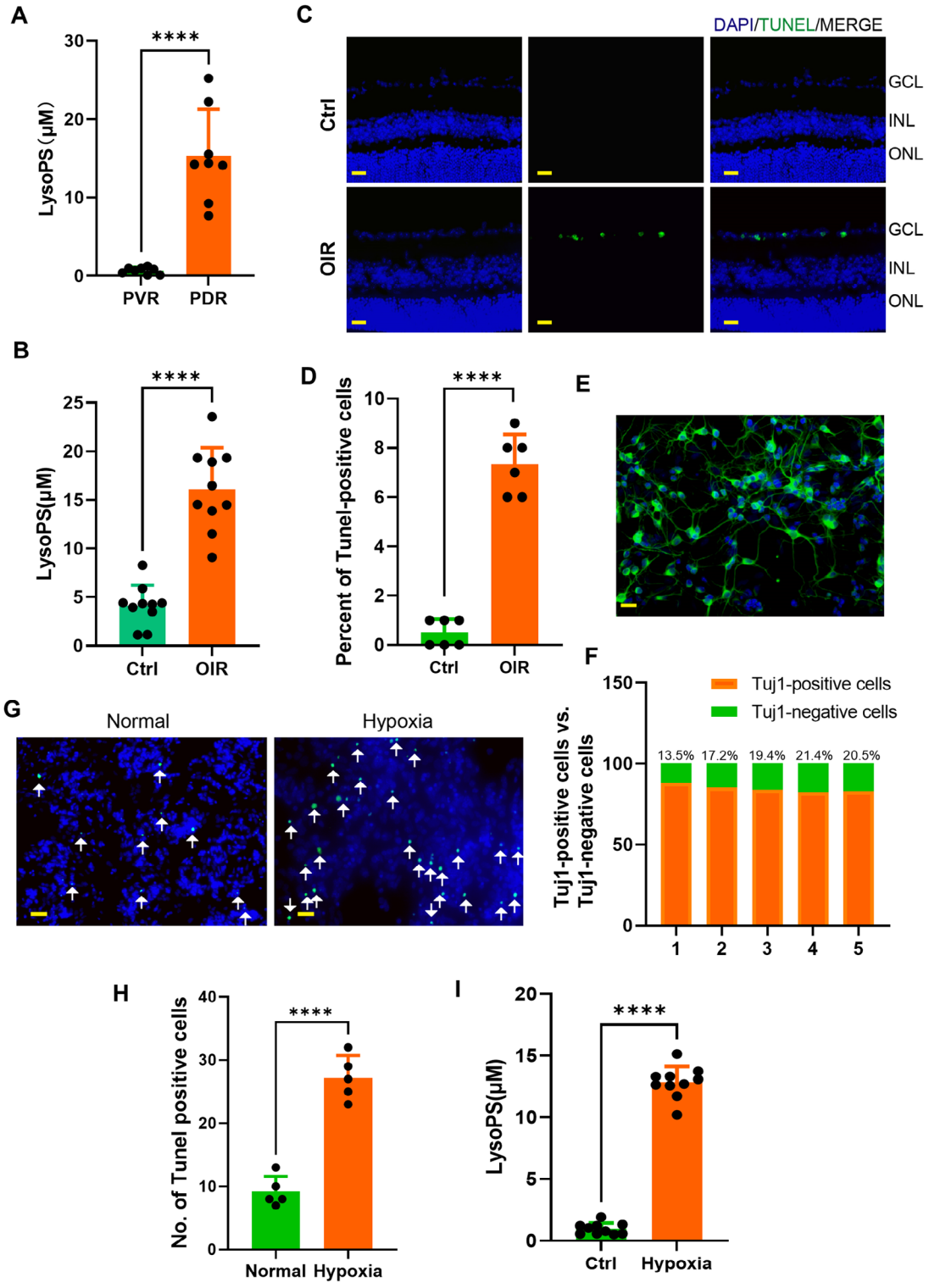

Fig. 1 Quantification of LysoPS in vitreous fluids and isolated ganglion cells. (**A**) LysoPS levels in vitreous fluids collected from PDR and PVR patients were quantified using a relative ELISA kit ($n=8$). (**B**) LysoPS levels in vitreous fluids collected from OIR mice and control mice were quantified ($n=10$). (**C**, **D**) apoptotic cells in the retinal tissues of OIR mice were detected using TUNEL staining ($n=6$). The following retinal layers are indicated: GCL, ganglion cell layer; INL, inner nuclear layer; and ONL, outer nuclear layer. (**E**, **F**) ganglion cells were isolated from the retinal tissues of OIR mice and characterised by Tuj1 staining ($n=5$). (**G**, **H**) isolated ganglion cells were subjected to hypoxic conditions, and apoptotic cells were quantified using a TUNEL assay. The total cells plated were labelled using a dUTP notch. The number of apoptotic cells was calculated ($n=5$). (**I**) LysoPS levels in the supernatants of primary ganglion cell cultures were quantified ($n=10$). The results are presented as the mean ± SD, ****$p<0.0001$; Student's *t* test; scale bar, 20 μm in (**C**) and (**E**), 50 in μm (**G**)

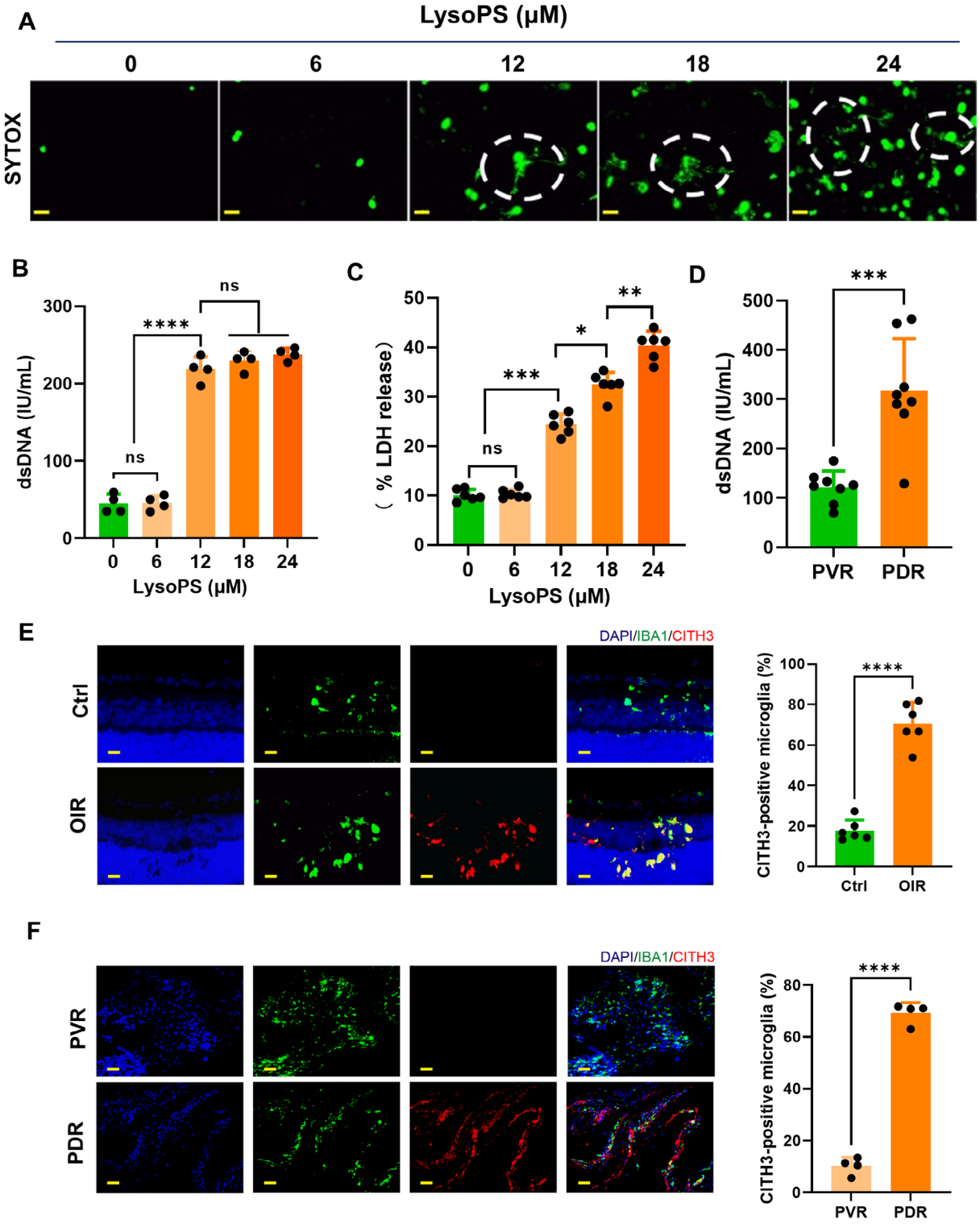

Fig. 2 LysoPS-induced extracellular traps in microglia. (**A**) HMC3 cells were treated with LysoPS as indicated, and extracellular traps were detected by SYTOX Green staining. White circles indicate cellular changes associated with filamentous DNA and membrane rupture. (**B**, **C**) dsDNA and LDH levels in cell supernatants were quantified ($n=4$). (**D**) dsDNA levels in the vitreous fluids from PDR and PVR patients were quantified using an ELISA kit ($n=8$). (**E**, **F**) the extracellular trap marker CITH3 was colocalised with microglial marker IBA1 in isolated retinal tissues from OIR mice and control mice (**E**, $n=6$), and in the fibrovascular membranes derived from PDR and PVR patients (**F**, $n=4$). The results are presented as the mean ± SD, *$p<0.05$, **$p<0.01$, ***$p<0.001$, ****$p<0.0001$, ns, no significance; Student's *t* test in (**D**), (**E**), and (**F**), one-way ANOVA in (**B**) and (**C**); scale bar, 50 μm in (**A**), 20 μm in (**E**) and (**F**)

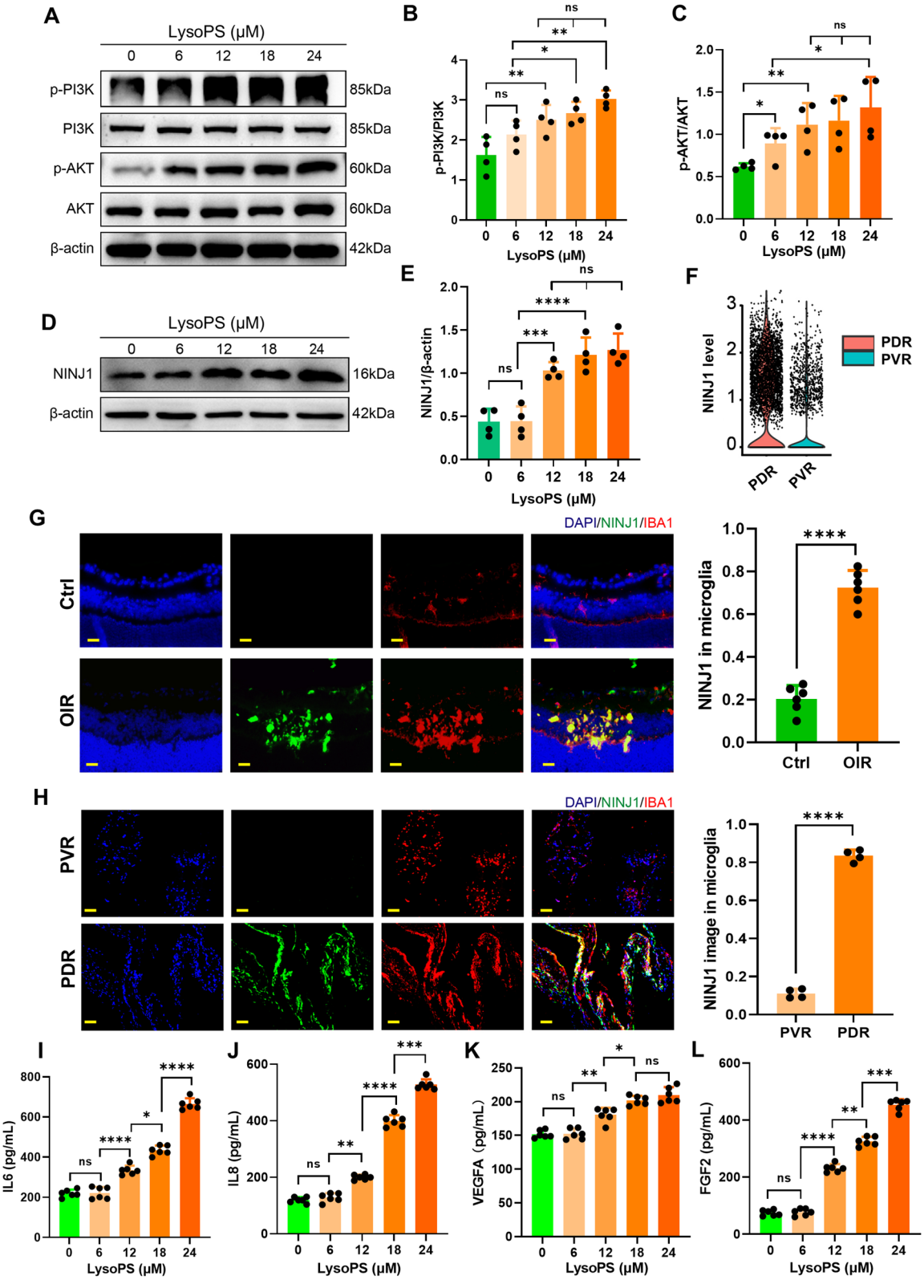

Fig. 3 (See legend on next page.)

(See figure on previous page.)

Fig. 3 LysoPS activated the PI3K-AKT pathway and NINJ1 in microglia (**A**) HMC3 cells were treated with LysoPS as indicated. Protein levels of PI3K, AKT, and their phosphorylated forms were quantified by immunoblotting. (**B**, **C**) the phosphorylated forms relative to the protein levels were normalised with β-actin ($n=4$). (**D**, **E**) the NINJ1 levels in LysoPS-treated HMC3 cells were measured by immunoblotting (**D**) and normalised with β-actin (**E**, $n=4$). (**F**) the expression profiles of NINJ1 in the microglia of PDR and PVR patients were analysed using T-SNE. (**G**, **H**). NINJ1 was colocalised with microglial marker IBA1 in retinal tissues isolated from OIR mice and control mice (**G**, $n=6$), and in fibrovascular membranes derived from PDR patients and PVR patients (**H**, $n=4$). (**I**–**L**) after LysoPS treatment, the levels of IL-6 (**I**), IL-8 (**J**), VEGFA (**K**), and FGF2 (**L**) in HMC3 cell supernatants were quantified using the relative ELISA kits ($n=4$). The results are presented as the mean ± SD, *$p<0.05$, **$p<0.01$, ***$p<0.001$, ****$p<0.0001$, ns, no significance; Student's *t* test in (**G**, **H**), one-way ANOVA in (**B**, **C**, **E**, **I**-**L**); scale bar, 20 μm in (**G**, **H**)

containing endothelial cells were cocultured with supernatants from LysoPS-treated mouse BMDM cells. Notably, LysoPS treatment significantly enhanced the choroid endothelial cell sprouting capacity compared to the untreated control (Fig. 4E, F). These findings suggest that LysoPS may contribute to the pathogenesis of DR by stimulating microglial inflammation.

Inhibition of GPR34, PI3K, and NINJ1 alleviated the effects of LysoPS

To determine if LysoPS induces microglial extracellular trap formation through NINJ1 activation, NINJ1 expression was silenced in HMC3 cells using a lentiviral vector carrying shRNA specifically targeting NINJ1 (Fig. 5A, B). Furthermore, LysoPS-treated HMC3 cells were treated with a GPR34 antagonist (GPR34-ANT) or a PI3K inhibitor (LY294002) to inhibit the effects of LysoPS. The results showed that LysoPS significantly upregulated the expression of NINJ1 and phosphorylated PI3K-AKT. However, these effects were attenuated by silencing NINJ1 or inhibiting GPR34 and PI3K. Notably, although GPR34 and PI3K inhibition suppressed NINJ1 expression, NINJ1 silencing did not affect PI3K-AKT phosphorylation (Fig. 5C–F), suggesting that NINJ1 may act as a downstream effector prompting microglia extracellular trap formation under inflammatory conditions.

To further investigate extracellular trap formation, NINJ1-silenced HMC3 cells were treated with LysoPS. As shown in Fig. 2A, although LysoPS strongly induced extracellular traps, silencing NINJ1 effectively negated this effect, with no changes observed in dsDNA and LDH levels (Fig. S3A–C). Additionally, inhibiting GPR34 and PI3K effectively prevented LysoPS-induced extracellular trap formation (Fig. S3D–F). Similarly, silencing NINJ1 and inhibiting PI3K-AKT signalling were able to eliminate LysoPS-induced microglial cytokine production (Fig. S4A–D). Furthermore, HRVEC cells were cocultured with HMC3 cell supernatants to determine the effects of NINJ1 and PI3K-AKT signalling on endothelial cell angiogenesis. As expected, silencing NINJ1 and inhibiting GPR34 and PI3K prevented LysoPS-induced cell proliferation, migration, and tubbing (Fig. 5G–J). These results suggest that inhibiting the GPR34-PI3K-AKT-NINJ1 axis is crucial for mitigating LysoPS-induced retinal neovascularisation.

Previous studies have shown that NINJ1 oligomerisation compromises cell membrane integrity. Thus, inhibiting this process could protect the cell membrane structure from inflammation-induced injury [33, 35, 36]. To determine the role of NINJ1 oligomerisation in microglial extracellular trap formation, the effect of LysoPS on NINJ1 oligomerisation was assessed using a BS3 crosslinker assay. As anticipated, LysoPS dose-dependently increased NINJ1 oligomerisation in HMC3 cells (Fig. S4E), and the effect was reversed by inhibiting the GPR34-PI3K-AKT-NINJ1 axis (Fig. S4F). Furthermore, the GPR34-PI3K-AKT-NINJ1 axis enhancing endothelial cell angiogenesis was examined. Supernatants derived from LysoPS-treated HMC3 cells induced HRVEC cell sprouting (Fig. S5A-C), and the effect of LysoPS on cell sprouting was eliminated by inhibiting the GPR34-PI3K-AKT-NINJ1 axis (Fig. S5D-F), suggesting that LysoPS induces neovascularisation by activating the GPR34-PI3K-AKT-NINJ1 axis in microglia.

Validation of LysoPS-induced retinal neovascularisation in vivo

To further validate the role of NINJ1 in vivo, shNINJ1 was cloned into an adeno-associated virus (AAV) vector. Following intravitreal injection of the AAV, the efficiency of NINJ1 silencing was established in the retinal tissues of mice (Fig. 6A, B). Subsequently, LysoPS, GPR34-ANT, or PI3K inhibitor was intravitreally injected into the mice, followed by the OIR procedure. The excised retinal tissues were then imaged to examine neovascular and avascular areas. Retinal neovascularisation was significantly increased in OIR mice compared to control mice, with LysoPS injection significantly enhancing angiogenic activity. However, inhibiting the GPR34-PI3K-AKT-NINJ1 axis significantly attenuated retinal neovascularisation (Fig. 6C–E). Similarly, retinal levels of IL-8, IL-6, VEGFA, and FGF2 were increased by LysoPS and decreased by inhibiting the GPR34-PI3K-AKT-NINJ1 axis (Fig. 6F–I).

To evaluate the clinical implication of this finding, retinal fibrovascular membranes were isolated from patients in the early stages of PDR and cocultured in an endothelial cell-specific medium. Endothelial cells isolated from these membranes were characterised using flow cytometry with an endothelial marker CD31 antibody (Fig. 7A, B). The excised retinal fibrovascular membranes were

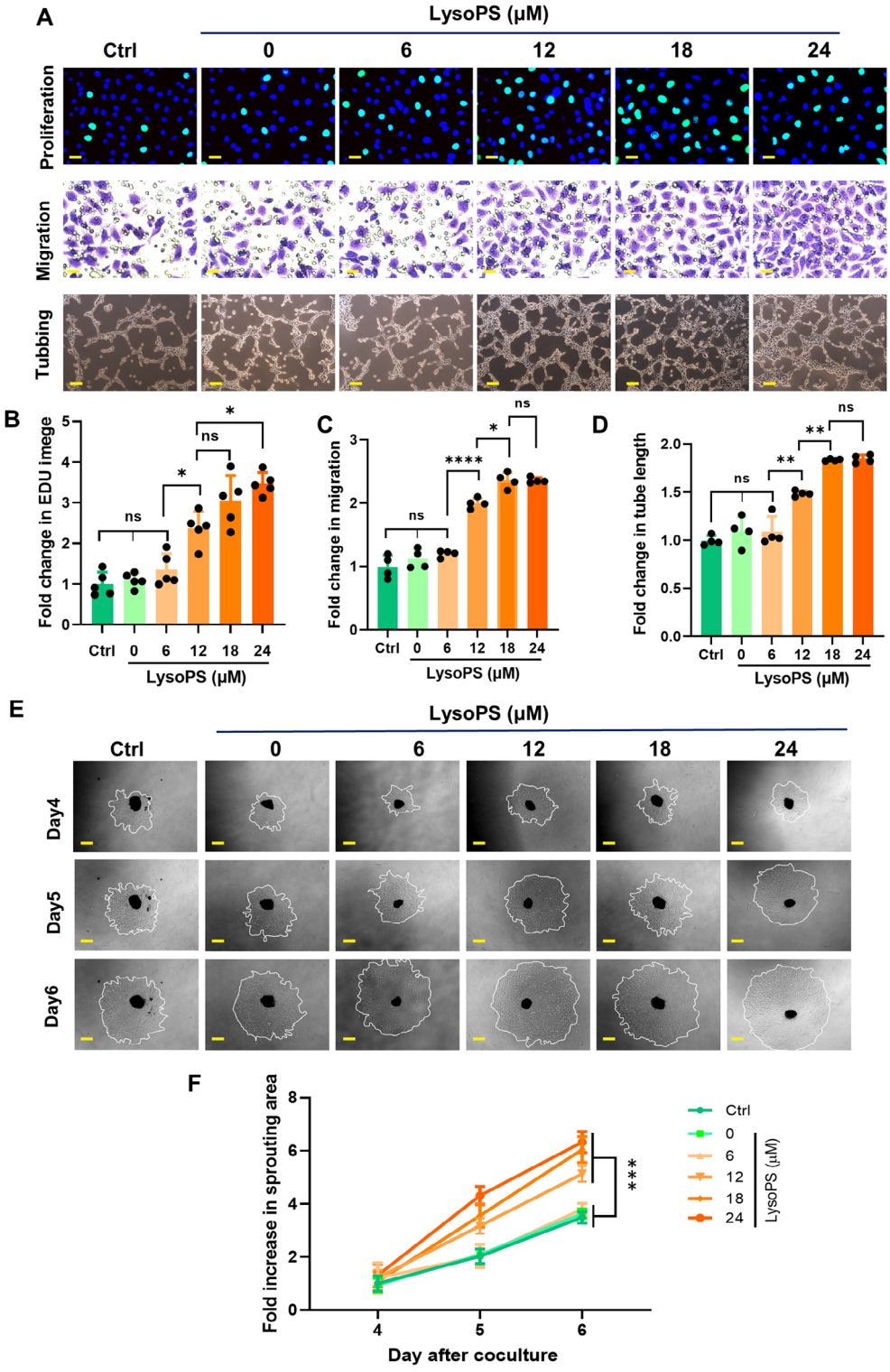

Fig. 4 LysoPS-induced retinal neovascularization (**A**) HRVEC cells were cocultured with supernatants from LysoPS-treated HMC3 cells as indicated. HRVEC cell proliferation was measured using an EdU assay (upper panel, 20 μm), cell migration was quantified using a transwell assay (middle panel, 20 μm), and the cell tube formation was imaged (lower panel, 100 μm). (**B**–**D**) the cell proliferation rate (**B**), cell migration rate (**C**), and cell tube formation (**D**) were calculated ($n=4$). (**E**, **F**) mouse BMDM cells were treated with LysoPS as indicated. Choroid membranes isolated from mice were treated with the supernatants collected from LysoPS-treated BMDM cells. Endothelial cell sprouting in the choroid membranes was imaged on days 4–6 using an inverted microscope (E, 200 μm), and the relative sprouting area was quantified (**F**, $n=4$). The results are presented as the mean ± SD, *$p<0.05$, **$p<0.01$, ***$p<0.001$, ****$p<0.0001$, ns, no significance; two-way ANOVA

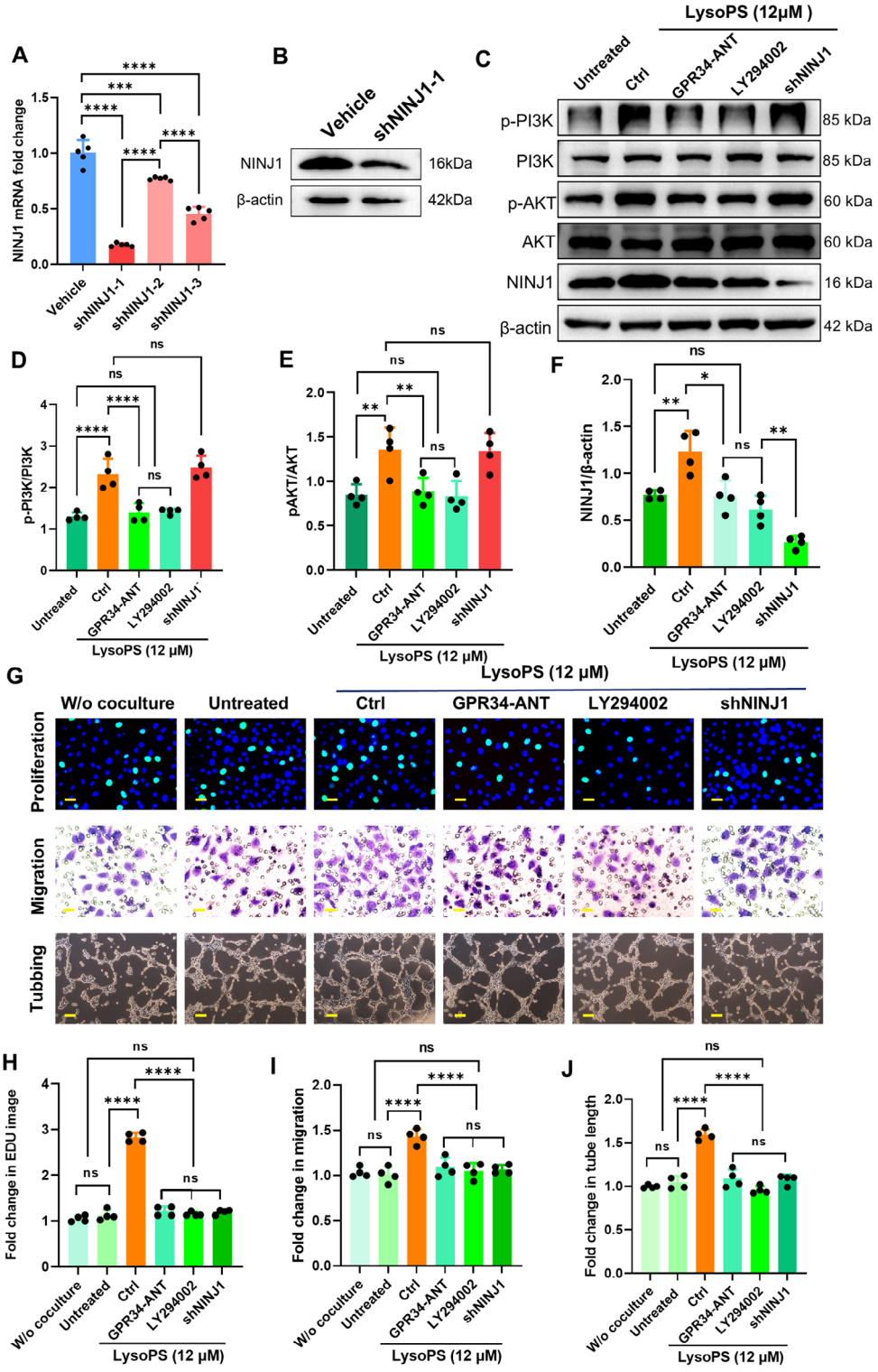

Fig. 5 Inhibition of LysoPS-activated microglial inflammation (**A**, **B**) NINJ1 was silenced in HMC3 cells using a lentiviral shNINJ1 and selected by RT-qPCR (A, $n=5$), and clone 1 was confirmed by immunoblotting (**B**). (**C**) in addition to NINJ1 silencing, HMC3 cells were treated with a GPR34 antagonist (GPR34-ANT) and a PI3K inhibitor (LY294002). The levels of NINJ1, PI3K, AKT, and their phosphorylated forms were quantified by immunoblotting. (**D**–**F**) the fold changes in the relative protein levels were calculated ($n=4$). (**G**–**J**) cell supernatants collected from the treated HMC3 cells were cocultured with HRVEC cells to determine cell phenotypic changes, including cell proliferation (upper panel, 20 μm), cell migration (middle panel, 20 μm), and tube formation (lower panel, 100 μm). The results are presented as the mean ± SD, *$p<0.05$, **$p<0.01$, ***$p<0.001$, ****$p<0.0001$, ns, no significance; one-way ANOVA in (**D**–**F**), two-way ANOVA in (**H**–**J**)

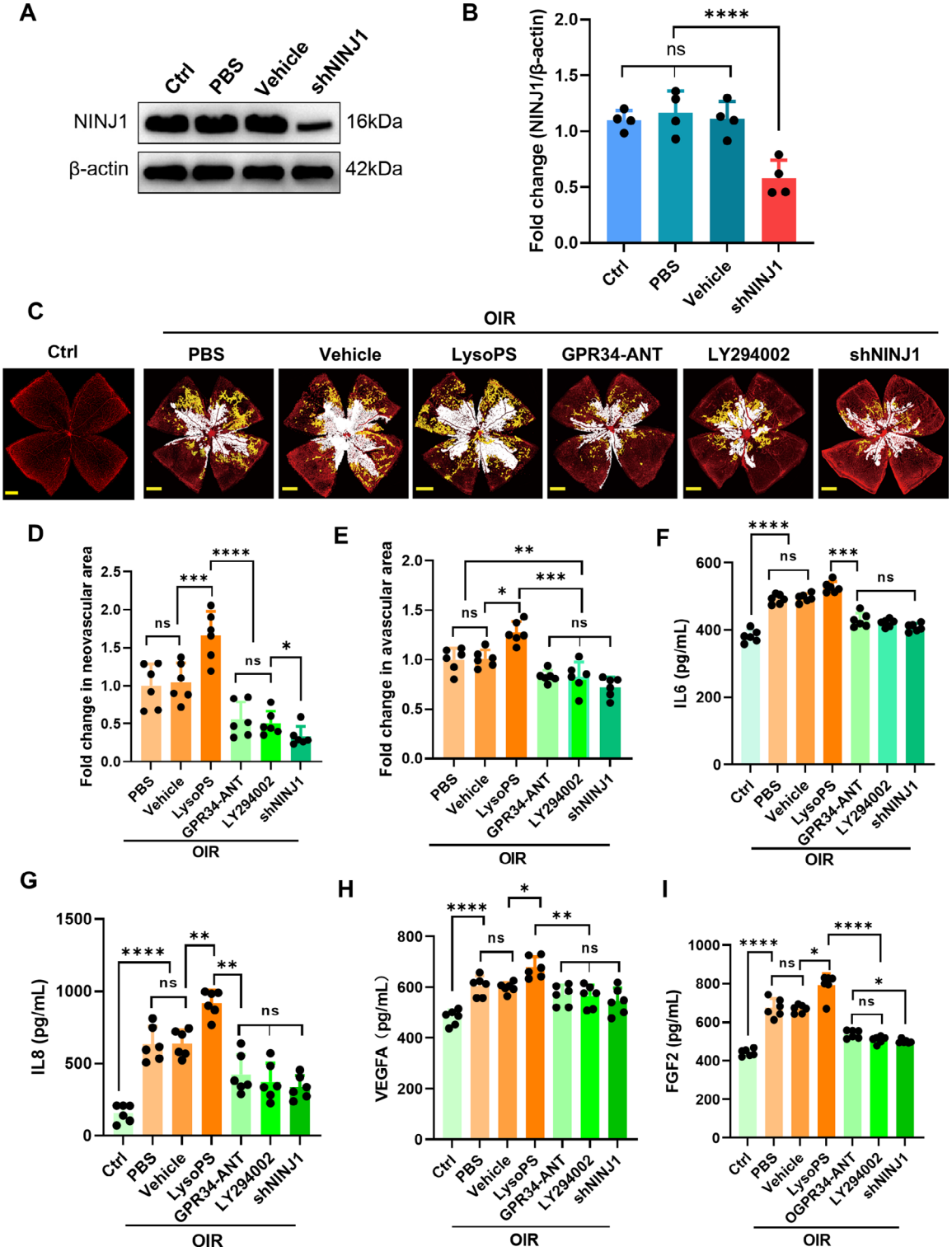

Fig. 6 Prevention of LysoPS-induced inflammation in OIR (**A**, **B**) AAV-carried shNINJ1 was intravitreally injected into OIR mice, and the efficiency of NINJ1 silencing in retinal tissues was confirmed by immunoblotting ($n=4$). (**C**) following AAV injection, further intravitreal injections of LysoPS, GPR34-ANT, or LY294002 were into OIR mice. Retinal tissue slides were imaged, with yellow areas indicating neovascularisation and white areas representing avascular regions. (**D**, **E**) the neovascular and avascular areas were quantified ($n=6$). (**F**–**I**) relative cytokines levels were quantified using relative ELISA kits ($n=6$). The results are presented as the mean ± SD, $^{*}p<0.05$, $^{**}p<0.01$, $^{***}p<0.001$,$^{****}p<0.0001$, ns, no significance; one-way ANOVA in (**B**), two-way ANOVA in (**D**–**I**); scale bar, 200 μm in (**C**)

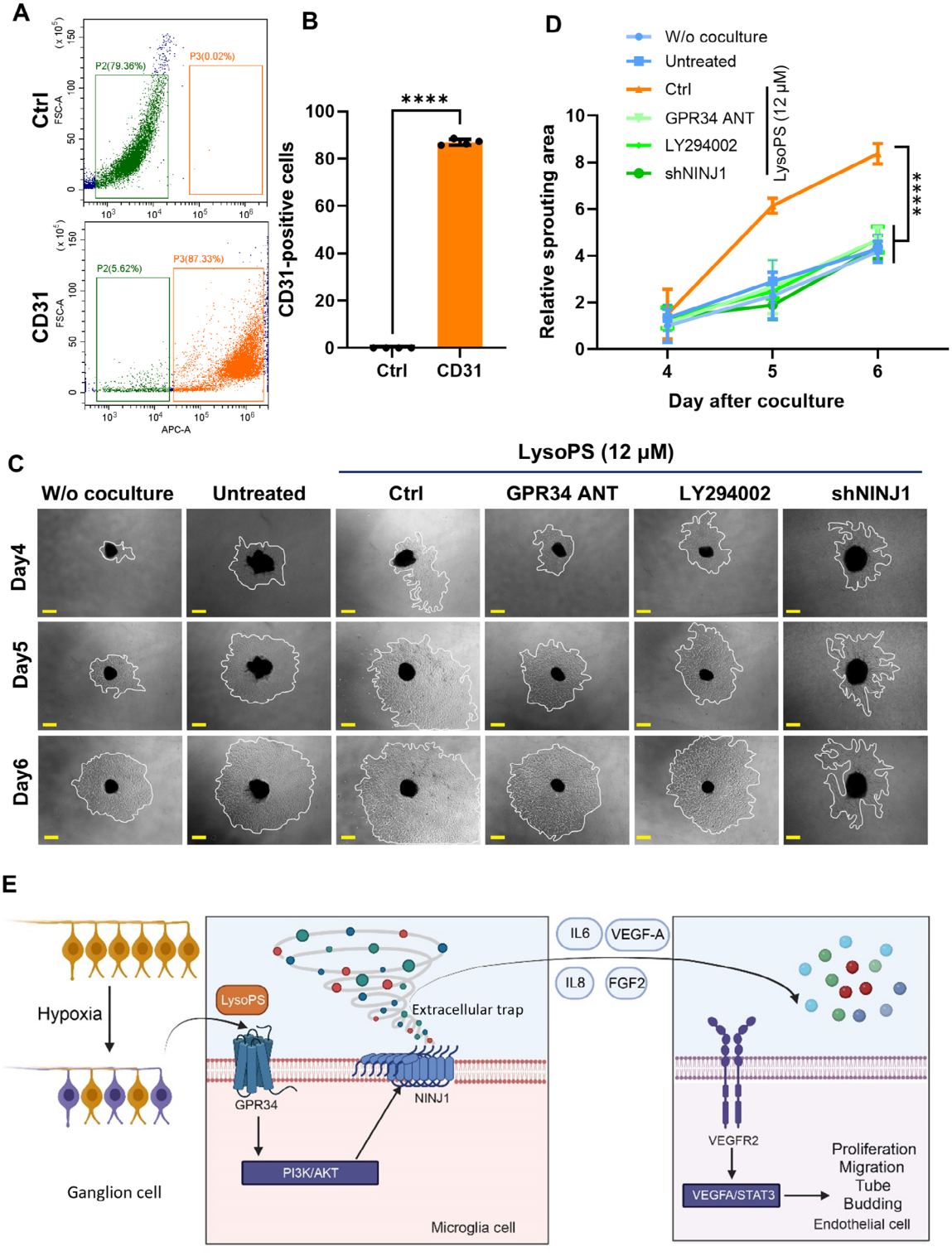

Fig. 7 Suppression of retinal neovascularisation by inhibiting the GPR34-PI3K-AKT-NINJ1 axis (**A**, **B**) Retinal endothelial cells were isolated from the fibrovascular membranes of PDR patients and cultured in an endothelial-specific medium. The purity of the cultured endothelial cells was analysed using flow cytometry with an endothelial marker CD31 antibody ($n=4$). (**C**, **D**) the fibrovascular membranes were treated with supernatants collected from LysoPS-treated HMC3 cells. To inhibit the effect of LysoPS, the HMC3 cells were pretreated with GPR34-ANT, LY294002, or shNINJ1. The relative sprouting rate of the endothelial cells within the fibrovascular membranes was evaluated on the specified days, as described in Fig. 4E, F ($n=4$). (**E**) schematic representation of the proposed mechanistic interaction among ganglion cells, microglia, and endothelial cells in promoting retinal neovascularisation. The results are presented as the mean ± SD, ****$p<0.0001$, Student's *t* test in (**B**), two-way ANOVA in (**D**); scale bar, 200 μm in (**C**)

then cocultured with LysoPS-induced HMC3 supernatants. As expected, LysoPS significantly enhanced fibrovascular membrane sprouting; however, this effect was reversed by inhibiting GPR34, PI3K, and NINJ1 in microglial cells (Fig. 7C, D). Additionally, LysoPS significantly increased the levels of VEGFA, phosphorylated VEGFR2, and STAT3. Inhibiting the GPR34-PI3K-AKT-NINJ1 axis effectively mitigated the effect of LysoPS on the activation of the VEGF-STAT3 pathway, which is essential for promoting endothelial cell angiogenesis (Fig. S6 A–D). Overall, this study introduces a novel concept, demonstrating that apoptotic ganglion cells induce retinal neovascularisation by activating the GPR34-PI3K-AKT-NINJ1 axis in microglia, as described in Fig. 7E.

Discussion

Retinal neurovascular disorders, characterised by neurodegeneration and vascular dysfunction, pose significant clinical challenges, and their underlying mechanisms remain elusive. Recent studies suggest that hypoxia, resulting from retinal hypoperfusion and endothelial glycolysis-induced lactic acid accumulation, triggers an angiogenic response in the microglia [15, 37]. Retinal microglia are essential for maintaining the integrity of the retinal neurovascular unit, and dysfunction of these cells may contribute to the progression of DR [38–40]. Ganglion cell injury has been implicated in the development of microglial dysfunction [41, 42]. This study further investigated the integration of ganglion cells, microglia, and vascular endothelial cells in the development of PDR. Our results revealed that LysoPS, a signalling molecule released from ganglion cells, stimulates microglia extracellular trap formation, and ultimately drives retinal neovascularisation. Notably, during the progression of the disease, increased levels of inflammation facilitated interaction among these three cell types in the retinal microenvironment.

Mounting studies have shown that inflammation is crucial to the progression of PDR. Proinflammatory cytokines such as FGF2, ANG, HGF, and VEGF are key mediators of retinal neovascularisation [15, 43–45]. This study revealed that LysoPS upregulates intraocular cytokines, including IL6, IL8, VEGFA, and FGF2, through interaction with the GPR34 receptor and activation of the PI3K-AKT pathway. In the mouse OIR model, the hyperoxic condition induced ischemia and vascular degradation due to increased apoptosis. Presumably, oxidative stress-induced ganglion cell injury is an early event in a cascade leading to increased cytokine production, retinal microglial extracellular trap formation, and retinal neovascularisation. Notably, LysoPS released from apoptotic ganglion cells served as a crucial microenvironmental factor for activating the GPR34-PI3K-AKT-NINJ1 axis, leading to retinal neovascularisation.

LysoPS, a potent inflammation inducer, has been implicated in gastrointestinal tract inflammation and vascular disorders, such as colitis and atherosclerosis [46, 47]. It also contributes to the progression of asthma by stimulating eosinophil extracellular trap formation [16, 48]. Furthermore, LysoPS influences several physiological processes, including mast cell degranulation, regulation of CD86 in B cells, and modulation of Rho in T cells [49–51]. GPR34, a receptor of LysoPS, is highly expressed in microglia, and its absence has been shown to impair microglial localisation to sites of neuronal injury, affecting their morphology and phagocytic activity [27]. This study demonstrated that LysoPS interacts with GPR34 and amplifies inflammatory response by activating the PI3K-AKT signalling pathway. This activation led to microglial extracellular trap formation and increased production of inflammatory cytokines, including IL6, IL8, VEGFA, and FGF2. It has been shown that senescent vasculature can prompt neutrophils to release extracellular traps, facilitating the clearance of damaged vessels and promoting vascular remodelling [52]. However, pathologic retinal neovascularisation induced by high levels of cytokines is inadequate for supplying sufficient blood and oxygen to neurons compared to normal vessels. This study found that LysoPS-induced inflammation triggered microglial extracellular trap formation, contributing to the development of leak-prone retinal neovascularisation and exacerbating tissue damage.

NINJ1, a 16 kDa transmembrane protein activated in response to nerve injury, has been identified as a key modulator in macrophage activation, neutrophil infiltration, and processes associated with vascular degeneration and neovascular permeability [53, 54]. Additionally, NINJ1 contributes to membrane lysis following macrophage death [33, 55]. Inhibition of NINJ1 oligomerisation with monoclonal antibodies has been shown to reduce tissue injury in hepatic ischemia-reperfusion models [33, 56]. This study further elucidated the role of NINJ1 oligomerisation in membrane lysis, by demonstrating its capacity to induce microglial extracellular trap formation. NINJ1 was identified as a key factor in microglial membranolysis, amplifying the inflammatory response and contributing to retinal neovascularisation. Consequently, targeting and inhibiting NINJ1 could be a potential therapeutic strategy for managing retinal neovascularisation. However, the precise mechanisms underlying NINJ1 oligomerisation induced by LysoPS in microglia remain elusive and require further investigation.

Conclusion

This study reveals that LysoPS derived from apoptotic retinal ganglion cells, stimulates the PI3K-AKT-activated microglial inflammatory response by interacting with the GPR34 receptor. This interaction subsequently led to the

activation of NINJ1, thereby promoting microglial extracellular trap formation and enhancing retinal neovascularisation. Inhibiting NINJ1 activation attenuated retinal neovascularisation by suppressing the effects of LysoPS on both microglial extracellular trap formation and cytokine production. These findings collectively showed that the GPR34-PI3K-AKT-NINJ1 axis played a crucial role in microglial extracellular trapping and subsequent retinal neovascularisation. Insight into the pathogenesis of PDR suggests a potential therapeutic approach for PDR intervention by suppressing LysoPS.

Supplementary Information

The online version contains supplementary material available at https://doi.org/10.1186/s12974-024-03265-7.

Supplementary Material 1

Supplementary Material 2

Author contributions

LC and JY conceived and designed the study. LC, HZ, YS, and YC performed experiments and data analysis. LC and YZ performed bioinformatics analysis. LC, MW, and YX interpreted data and wrote manuscript drafts and revisions. XL and YX administrated experiments. YX and JY supervised the project. LC and YX wrote and edited the manuscript. All authors agree on the manuscript's content and approve the submission.

Funding

This study was supported by the National Natural Science Foundation of China Research Grants (No. Nos. 82271107).

Data availability

No datasets were generated or analysed during the current study.

Declarations

Ethical approval

The experiments using the clinical samples were approved by the Ethics Committee of the Eye Hospital of Nanjing Medical University (protocol No. 2021011), with written informed consent obtained from the patients enrolled in this study. Animal experiments were performed according to the Institutional Animal Care and Use guidelines approved by the Nanjing Medical University Research Committee (No.IACUC-2407047).

Competing interests

The authors declare no competing interests.

Received: 14 August 2024 / Accepted: 18 October 2024
Published online: 28 October 2024

References

1. Selvam S, Kumar T, Fruttiger M. Retinal vasculature development in health and disease. Prog Retin Eye Res. 2018;63:1–19.
2. Semeraro F, Morescalchi F, Cancarini A, Russo A, Rezzola S, Costagliola C. Diabetic retinopathy, a vascular and inflammatory disease: therapeutic implications. Diabetes Metab. 2019;45:517–27.
3. Fevereiro-Martins M, Marques-Neves C, Guimarães H, Bicho M. Retinopathy of prematurity: a review of pathophysiology and signaling pathways. Surv Ophthalmol. 2023;68:175–210.
4. Hayreh SS. Photocoagulation for retinal vein occlusion. Prog Retin Eye Res. 2021;85:100964.
5. Wong TY, Cheung CMG, Larsen M, Sharma S, Simó R. Diabetic retinopathy. Nat Rev Dis Primers. 2016;2:16012.
6. Hammes H-P, Feng Y, Pfister F, Brownlee M. Diabetic Retinopathy: Targeting Vasoregression. Diabetes. 2011;60:9–16.
7. Alarcon-Martinez L, Shiga Y, Villafranca-Baughman D, Cueva Vargas JL, Vidal Paredes IA, Quintero H, et al. Neurovascular dysfunction in glaucoma. Prog Retin Eye Res. 2023;97:101217.
8. Simó R, Hernández C, European Consortium for the Early Treatment of Diabetic Retinopathy (EUROCONDOR). Neurodegeneration in the diabetic eye: new insights and therapeutic perspectives. Trends Endocrinol Metab. 2014;25:23–33.
9. Uemura A, Fruttiger M, D'Amore PA, De Falco S, Joussen AM, Sennlaub F, et al. VEGFR1 signaling in retinal angiogenesis and microinflammation. Prog Retin Eye Res. 2021;84:100954.
10. Huang H. Pericyte-endothelial interactions in the retinal microvasculature. Int J Mol Sci. 2020;21:7413.
11. Wang W, Lo ACY. Diabetic Retinopathy: pathophysiology and treatments. Int J Mol Sci. 2018;19:E1816.
12. Cheung N, Mitchell P, Wong TY. Diabetic retinopathy. Lancet. 2010;376:124–36.
13. Kinuthia UM, Wolf A, Langmann T. Microglia and inflammatory responses in Diabetic Retinopathy. Front Immunol. 2020;11:564077.
14. Li Q, Barres BA. Microglia and macrophages in brain homeostasis and disease. Nat Rev Immunol. 2018;18:225–42.
15. He C, Liu Y, Huang Z, Yang Z, Zhou T, Liu S, et al. A specific RIP3 + subpopulation of microglia promotes retinopathy through a hypoxia-triggered necroptotic mechanism. Proc Natl Acad Sci U S A. 2021;118:e2023290118.
16. Lu Y, Huang Y, Li J, Huang J, Zhang L, Feng J, et al. Eosinophil extracellular traps drive asthma progression through neuro-immune signals. Nat Cell Biol. 2021;23:1060–72.
17. Agrawal I, Sharma N, Saxena S, Arvind S, Chakraborty D, Chakraborty DB, et al. Dopamine induces functional extracellular traps in microglia. iScience. 2021;24:101968.
18. Conedera FM, Kokona D, Zinkernagel MS, Stein JV, Lin CP, Alt C, et al. Macrophages coordinate immune response to laser-induced injury via extracellular traps. J Neuroinflammation. 2024;21:68.
19. Papayannopoulos V. Neutrophil extracellular traps in immunity and disease. Nat Rev Immunol. 2018;18:134–47.
20. Herre M, Cedervall J, Mackman N, Olsson A-K. Neutrophil extracellular traps in the pathology of cancer and other inflammatory diseases. Physiol Rev. 2023;103:277–312.
21. Clark M, Kim J, Etesami N, Shimamoto J, Whalen RV, Martin G, et al. Group A Streptococcus prevents mast cell degranulation to promote extracellular trap formation. Front Immunol. 2018;9:327.
22. Yousefi S, Morshed M, Amini P, Stojkov D, Simon D, von Gunten S, et al. Basophils exhibit antibacterial activity through extracellular trap formation. Allergy. 2015;70:1184–8.
23. O'Neil LJ, Oliveira CB, Wang X, Navarrete M, Barrera-Vargas A, Merayo-Chalico J, et al. Neutrophil extracellular trap-associated carbamylation and histones trigger osteoclast formation in rheumatoid arthritis. Ann Rheum Dis. 2023;82:630–8.
24. Chen L, Zhao Y, Lai D, Zhang P, Yang Y, Li Y, et al. Neutrophil extracellular traps promote macrophage pyroptosis in sepsis. Cell Death Dis. 2018;9:597.
25. Döring Y, Soehnlein O, Weber C. Neutrophil Extracellular traps in atherosclerosis and Atherothrombosis. Circ Res. 2017;120:736–43.
26. Zhao Y, Hasse S, Bourgoin SG. Phosphatidylserine-specific phospholipase A1: a friend or the devil in disguise. Prog Lipid Res. 2021;83:101112.
27. Lou L, Yu T, Dai Y, Zhao S, Feng S, Xu J, et al. Mafba and Mafbb regulate microglial colonization of zebrafish brain via controlling chemotaxis receptor expression. Proc Natl Acad Sci U S A. 2022;119:e2203273119.
28. Ikubo M, Inoue A, Nakamura S, Jung S, Sayama M, Otani Y, et al. Structure-activity relationships of lysophosphatidylserine analogs as agonists of G-protein-coupled receptors GPR34, P2Y10, and GPR174. J Med Chem. 2015;58:4204–19.
29. Schöneberg T, Meister J, Knierim AB, Schulz A. The G protein-coupled receptor GPR34 - the past 20 years of a grownup. Pharmacol Ther. 2018;189:71–88.
30. Wang X, Cai J, Lin B, Ma M, Tao Y, Zhou Y, et al. GPR34-mediated sensing of lysophosphatidylserine released by apoptotic neutrophils activates type 3 innate lymphoid cells to mediate tissue repair. Immunity. 2021;54:1123–e11368.

31. Lee J-W, Nam H, Kim LE, Jeon Y, Min H, Ha S, et al. TLR4 (toll-like receptor 4) activation suppresses autophagy through inhibition of FOXO3 and impairs phagocytic capacity of microglia. Autophagy. 2019;15:753–70.
32. Wen Y, Chen X, Feng H, Wang X, Kang X, Zhao P, et al. Kdm6a deficiency in microglia/macrophages epigenetically silences Lcn2 expression and reduces photoreceptor dysfunction in diabetic retinopathy. Metabolism. 2022;136:155293.
33. Kayagaki N, Kornfeld OS, Lee BL, Stowe IB, O'Rourke K, Li Q, et al. NINJ1 mediates plasma membrane rupture during lytic cell death. Nature. 2021;591:131–6.
34. Araki T, Milbrandt J. Ninjurin, a novel adhesion molecule, is induced by nerve injury and promotes axonal growth. Neuron. 1996;17:353–61.
35. Degen M, Santos JC, Pluhackova K, Cebrero G, Ramos S, Jankevicius G, et al. Structural basis of NINJ1-mediated plasma membrane rupture in cell death. Nature. 2023;618:1065–71.
36. Kayagaki N, Stowe IB, Alegre K, Deshpande I, Wu S, Lin Z, et al. Inhibiting membrane rupture with NINJ1 antibodies limits tissue injury. Nature. 2023;618:1072–7.
37. Liu Z, Xu J, Ma Q, Zhang X, Yang Q, Wang L, et al. Glycolysis links reciprocal activation of myeloid cells and endothelial cells in the retinal angiogenic niche. Sci Transl Med. 2020;12:eaay1371.
38. Mills SA, Jobling AI, Dixon MA, Bui BV, Vessey KA, Phipps JA, et al. Fractalkine-induced microglial vasoregulation occurs within the retina and is altered early in diabetic retinopathy. Proc Natl Acad Sci U S A. 2021;118:e2112561118.
39. Phipps JA, Dixon MA, Jobling AI, Wang AY, Greferath U, Vessey KA, et al. The renin-angiotensin system and the retinal neurovascular unit: a role in vascular regulation and disease. Exp Eye Res. 2019;187:107753.
40. Meng C, Gu C, He S, Su T, Lhamo T, Draga D, et al. Pyroptosis in the retinal neurovascular unit: New insights into Diabetic Retinopathy. Front Immunol. 2021;12:763092.
41. Kumar S, Akopian A, Bloomfield SA. Neuroprotection of retinal ganglion cells suppresses Microglia activation in a mouse model of Glaucoma. Invest Ophthalmol Vis Sci. 2023;64:24.
42. Hu Z, Deng N, Liu K, Zhou N, Sun Y, Zeng W. CNTF-STAT3-IL-6 Axis mediates Neuroinflammatory Cascade across Schwann Cell-Neuron-Microglia. Cell Rep. 2020;31:107657.
43. Rangasamy S, Srinivasan R, Maestas J, McGuire PG, Das A. A potential role for angiopoietin 2 in the regulation of the blood-retinal barrier in diabetic retinopathy. Invest Ophthalmol Vis Sci. 2011;52:3784–91.
44. Cai W, Rook SL, Jiang ZY, Takahara N, Aiello LP. Mechanisms of hepatocyte growth factor-induced retinal endothelial cell migration and growth. Invest Ophthalmol Vis Sci. 2000;41:1885–93.
45. Rattner A, Williams J, Nathans J. Roles of HIFs and VEGF in angiogenesis in the retina and brain. J Clin Invest. 2019;129:3807–20.
46. Otake-Kasamoto Y, Kayama H, Kishikawa T, Shinzaki S, Tashiro T, Amano T, et al. Lysophosphatidylserines derived from microbiota in Crohn's disease elicit pathological Th1 response. J Exp Med. 2022;219:e20211291.
47. Nishikawa M, Kurano M, Ikeda H, Aoki J, Yatomi Y. Lysophosphatidylserine has bilateral effects on macrophages in the pathogenesis of atherosclerosis. J Atheroscler Thromb. 2015;22:518–26.
48. Kim HJ, Sim MS, Lee DH, Kim C, Choi Y, Park H, et al. Lysophosphatidylserine induces eosinophil extracellular trap formation and degranulation: implications in severe asthma. Allergy. 2020;75:3159–70.
49. Lloret S, Moreno JJ. Ca2 + influx, phosphoinositide hydrolysis, and histamine release induced by lysophosphatidylserine in mast cells. J Cell Physiol. 1995;165:89–95.
50. Wolf EW, Howard ZP, Duan L, Tam H, Xu Y, Cyster JG. GPR174 signals via Gαs to control a CD86-containing gene expression program in B cells. Proc Natl Acad Sci U S A. 2022;119:e2201794119.
51. Gurusamy M, Tischner D, Shao J, Klatt S, Zukunft S, Bonnavion R, et al. G-protein-coupled receptor P2Y10 facilitates chemokine-induced CD4 T cell migration through autocrine/paracrine mediators. Nat Commun. 2021;12:6798.
52. Binet F, Cagnone G, Crespo-Garcia S, Hata M, Neault M, Dejda A, et al. Neutrophil extracellular traps target senescent vasculature for tissue remodeling in retinopathy. Science. 2020;369:eaay5356.
53. Lee H-J, Ahn BJ, Shin MW, Choi J-H, Kim K-W. Ninjurin1: a potential adhesion molecule and its role in inflammation and tissue remodeling. Mol Cells. 2010;29:223–7.
54. Lee H-J, Ahn BJ, Shin MW, Jeong J-W, Kim JH, Kim K-W. Ninjurin1 mediates macrophage-induced programmed cell death during early ocular development. Cell Death Differ. 2009;16:1395–407.
55. David L, Borges JP, Hollingsworth LR, Volchuk A, Jansen I, Garlick E, et al. NINJ1 mediates plasma membrane rupture by cutting and releasing membrane disks. Cell. 2024;187:2224–e223516.
56. Hu Y, Zhan F, Wang Y, Wang D, Lu H, Wu C, et al. The Ninj1/Dusp1 Axis contributes to Liver Ischemia Reperfusion Injury by regulating macrophage activation and neutrophil infiltration. Cell Mol Gastroenterol Hepatol. 2023;15:1071–84.

Publisher's note